PHYSICAL REVIEW FLUIDS **2**, 063101 (2017)

Dumbbell formation for elastic capsules in nonlinear extensional Stokes flows

P. Dimitrakopoulos*

Department of Chemical and Biomolecular Engineering, University of Maryland, College Park, Maryland 20742, USA

(Received 12 December 2016; published 27 June 2017)

Cross-slot and four-roll-mill microdevices are commonly used for particle manipulation and characterization owing to the stagnation-point flow at the device center. Because of the solid boundaries, these devices may generate extensional Stokes flows where the velocity is a nonlinear function of position associated with a decreased pressure at the particle edges and an increased pressure at the particle middle. Our computational investigation shows that in this class of Stokes flows, an elastic capsule made of a strain-hardening membrane develops two distinct steady-state conformations at strong flows, i.e., an elongated weak dumbbell shape with rounded edges at low flow nonlinearity and a laterally extended dumbbell shape at high flow nonlinearity. These effects are more pronounced for the less strain-hardening capsules which develop a flat extended middle where the two sides of the membrane approach each other. The strong stability properties of the strain-hardening capsules (owing to the development of strong membrane tensions) contrast significantly with the behavior of droplets in these nonlinear flows which are unable to achieve highly deformed steady-state dumbbell shapes owing to their constant surface tension.

DOI: 10.1103/PhysRevFluids.2.063101

I. INTRODUCTION

The study of the interfacial dynamics of artificial or physiological capsules (i.e., membrane-enclosed fluid volumes) in Stokes flows has seen increased interest during the past few decades due to their numerous engineering and biomedical applications. Artificial capsules have wide applications in the pharmaceutical, food, and cosmetic industries [1]. In pharmaceutical processes, for example, capsules are commonly used for the transport of medical agents. In addition, the motion of red blood cells through vascular microvessels has long been recognized as a fundamental problem in physiology and biomechanics, since the main function of these cells, to exchange oxygen and carbon dioxide with the tissues, occurs in capillaries [2]. The aforementioned applications have motivated the study of artificial capsules in linear flows, such as simple shear and extensional flows, which reveal the fundamental capsule physics; e.g., see Refs. [3–6].

In our earlier papers [4,7,8], we studied computationally the dynamics of strain-hardening and strain-softening capsules in a (linear) planar extensional flow and showed that as the flow rate increases, all capsules reach elongated steady-state configurations but the cross section of the more strain-hardening capsules preserves its elliptical shape while the less strain-hardening capsules become lamellar. We also developed a scaling analysis for elongated strain-hardening capsules which provides physical insight on the extensional capsule dynamics [7]. In addition, we investigated the cusp formation at the capsule edges in planar extensional flows owing to a transition of the edge tensions from tensile to compressive [8,9].

In this paper, we investigate the capsule dynamics in extensional Stokes flows where the velocity is a nonlinear function of position, associated with a decreased pressure at the capsule edges and an increased pressure at the capsule middle. Such flows may be created owing to the presence of solid boundaries in industrial and physiological processes, e.g., in four-roll-mill and cross-slot microdevices and similar conformations of vascular capillaries [2,10–12]. In this paper, this class

*dimitrak@umd.edu

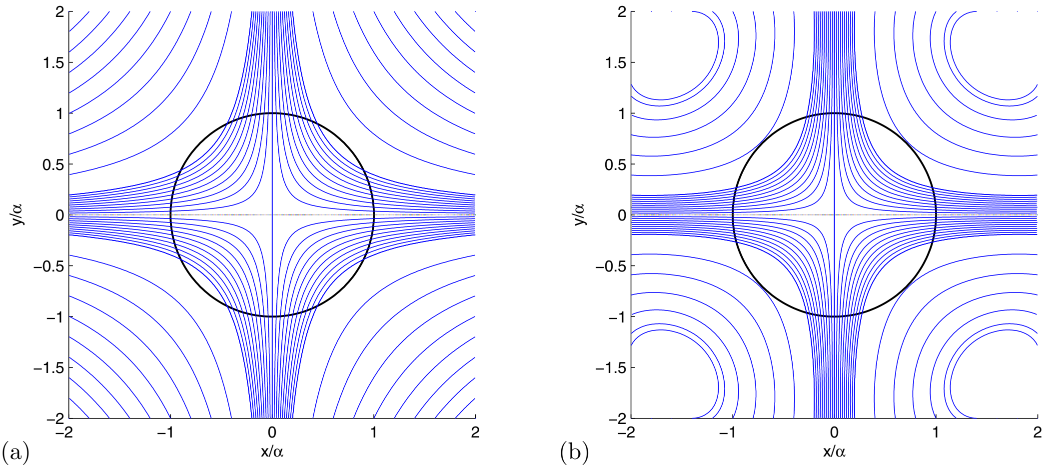

FIG. 1. Streamlines for the planar extensional flow given by Eq. (1) with (a) $b_A = 0$ and (b) $b_A = -0.1$. The streamlines have the same starting points at $y/a = -2,2$. A unit circle with zero origin is also shown for comparison reasons.

of negligible inertia flows are called nonlinear Stokes flows to distinguish them from the commonly used (linear) extensional flows.

Cross-slot and four-roll-mill microdevices are commonly used for particle manipulation and characterization owing to the stagnation-point flow at the device center [10–13]. Because of the solid boundaries, these devices may generate extensional flows where the velocity is a nonlinear function of position. This flow nonlinearity may have significant effects on the deformation of soft particles as their size increases, as revealed by earlier studies on two-dimensional and axisymmetric bubbles [14,15].

This type of extensional flows motivated us to investigate the capsule dynamics in Antanovskii's nonlinear extensional flow described by

$$u_x^\infty = Gx\left(1 + b_A\frac{x^2+3y^2}{a^2}\right), \quad u_y^\infty = -Gy\left(1 + b_A\frac{3x^2+y^2}{a^2}\right), \tag{1}$$

where G is the flow rate, a is the capsule size, and b_A is a dimensionless constant associated with the cubic flow term which adds a rotational velocity field [14,16]. The velocity described by Eq. (1) generates a pressure which varies with position as $p^\infty = p_0 + 6\mu G\, b_A(x^2 - y^2)/a^2$, while its streamlines for $b_A < 0$ are similar to that of the linear planar extensional flow (of $b_A = 0$), slightly pushed towards the stagnation point at the origin [14,15]. (See also Fig. 1.)

This flow field represents a class of extensional flows which accounts for the nonlinear variation of the flow velocity with position (e.g., due to the present of solid boundaries) via the simplest possible (i.e., cubic) polynomial, which is also the most fundamental [14]. We clarify that the extensional flows created in complicated cross-slot and four-roll-mill devices may be associated with positive or negative b_A [16]. For example, it was estimated that the larger droplets used in the four-roll-mill experiments of Taylor correspond to $b_A = 0.01$ [16,17]. The nonlinearity strength $|b_A|$ produced in a given geometry is increased as a^2 with the particle size since this is used in Eq. (1) as the length scale. Our work reveals that in a microfluidic cross junction constructed by two square channels, when the capsule size is smaller but comparable to the device size, the flow nonlinearity corresponds to $b_A = -O(0.1)$, as shown later in Fig. 14.

In our recent paper, we investigated the capsule dynamics for positive b_A which results in cusp formation [9]. In this work, we investigate the effects of increasing the flow nonlinearity for negative b_A, and thus for a decreased pressure at the capsule edges and an increased pressure at the capsule middle, which results in a dumbbell formation.

II. PROBLEM DESCRIPTION AND COMPUTATIONAL METHOD

We consider a three-dimensional spherical capsule with a thin elastic membrane in an infinite ambient fluid. The interior and exterior fluids are Newtonian, with viscosities $\lambda\mu$ and μ and the same density. The capsule size is specified by the radius a of its quiescent spherical shape of volume $V = 4\pi a^3/3$. Far away from the capsule, the flow approaches the undisturbed nonlinear planar extensional flow described by Eq. (1). We assume that the Reynolds number is small for both the surrounding and the inner flows, and thus the capsule deformation occurs in the Stokes regime, as in the four-roll-mill and cross-slot experiments of droplets and capsules [3,17–20].

Our membrane description is based on the well-established continuum approach and the theory of thin shells by considering the membrane as a two-dimensional continuum with shearing and area-dilatation resistance but negligible bending resistance. This modeling has been proven to represent a wide range of thin elastic membranes, whose thickness is several orders of magnitude smaller than the size of the capsules and their bending resistance is very small compared to their shearing resistance [4,5,21].

The surface stress is determined by the in-plane tensions

$$\Delta \boldsymbol{f} = -\nabla_s \cdot \boldsymbol{\tau} = -(\tau^{\alpha\beta}|_\alpha\, \boldsymbol{t}_\beta + b_{\alpha\beta}\, \tau^{\alpha\beta}\, \boldsymbol{n}), \tag{2}$$

where the Greek indices range over 1 and 2, while Einstein summation convention is employed for (every two) repeated indices. In this equation, the $\tau^{\alpha\beta}|_\alpha$ notation denotes covariant differentiation, $\boldsymbol{t}_\beta = \partial \boldsymbol{x}/\partial\theta^\beta$ are the tangent vectors on the capsule surface described with arbitrary curvilinear coordinates θ^β, and $b_{\alpha\beta}$ is the surface curvature tensor [4,5].

In this work, we mostly consider capsules made of strain-hardening membranes whose tensions growth superlinearly with the applied strains, and thus these capsules are able to withstand large deformations without membrane rupture [4,7]. In particular, the in-plane tension tensor $\boldsymbol{\tau}$ is described by the strain-hardening constitutive law of Skalak *et al.* [22], which relates $\boldsymbol{\tau}$'s eigenvalues (or principal elastic tensions $\tau_\beta^P, \beta = 1,2$) with the principal stretch ratios λ_β by

$$\tau_1^P = \frac{G_s \lambda_1}{\lambda_2}\{\lambda_1^2 - 1 + C\lambda_2^2[(\lambda_1\lambda_2)^2 - 1]\}. \tag{3}$$

Note that the reference shape of the elastic tensions is the spherical quiescent shape of the capsule while to calculate τ_2^P the λ_β subscripts are reversed. In Eq. (3), G_s is the membrane's shear modulus while the dimensionless parameter C describes the membrane hardness (i.e., the strength of its strain-hardening nature) and is associated with the scaled area-dilatation modulus G_a of the membrane, $G_a/G_s = 1 + 2C$ [22].

We emphasize that real capsules with thin membranes have a small bending resistance resulting from the membrane thickness. In particular, the theory of thin shells predicts that for an isotropic membrane, the bending modulus K_b is proportional to the (surface) shear modulus G_s and the square of the membrane thickness h, i.e., $K_b \sim G_s\, h^2$, and thus the scaled modulus is $K_b/(G_s\, a^2) \sim (h/a)^2$ [23]. For a typical relative thickness of $h/a = 10^{-2}$, the scaled modulus is $K_b/(G_s\, a^2) \sim 10^{-4}$, and thus the bending resistance is insignificant compared to the shearing and area-dilatation resistance for the overall capsule dynamics.

In this work, we investigate capsules with viscosity ratio $\lambda = 1$. We emphasize that at steady state there is no flow on the interfacial membrane or inside the capsule owing to the solid-material interface and the symmetry of the planar extensional flow, and thus the viscosity ratio λ does not affect the steady-state capsule shape. To explain this further, observe that the interfacial velocity should follow the symmetry of the planar extensional flow as shown in Fig. 1. For a viscous droplet where the interface is just a separation of two fluid phases with no material, this results in an inner circulation which follows the symmetry of the extensional flow. On the other hand, the material membrane of a capsule cannot satisfy the velocity pattern imposed by the planar extensional flow, and thus at steady state there is no flow on the interfacial membrane or inside the capsule.

Therefore, the present problem depends on three dimensionless parameters, the flow nonlinearity b_A, the capillary number $\mathrm{Ca} = \mu G a / G_s$, and the membrane hardness C. In our computations, we keep constant the fluid and capsule properties, μ, a, and G_s, and vary the flow rate G; thus the capillary number Ca can be regarded as a dimensionless flow rate. In this study, the capsule size a is used as the length scale, the curvatures are scaled with the curvature of the quiescent spherical capsule $\mathcal{C}^0_{xy} = \mathcal{C}^0_{zy} = a^{-1}$, the time scale is $t_f = G^{-1}$, and the membrane tensions are scaled with G_s.

The required flow rates for large capsule deformations shown in our work have been achieved under Stokes flow conditions for droplets and capsules in four-roll-mill and cross-slot experiments [17,19,20]. Large capsule deformations have been achieved in compression experiments and in cross-slot microfluidic elongation experiments, and the experimental findings have shown that the capsule dynamics can be well described by a single constitutive law with a fixed value of the employed moduli [20,21].

The numerical solution of the interfacial Stokes flow problem is achieved through our membrane spectral boundary element method, and the interested reader is referred to our earlier papers for more details on our spectral algorithm and the extensional dynamics of strain-hardening and strain-softening capsules [4,7,8]. For this study, we divided the capsule interface into mostly $N_E = 10$ spectral elements and utilized $N_B = 12$–18 spectral discretization points per direction on each element, i.e., a total of $N = N_E\, N_B^2 = 1440$–3240 spectral points. Convergence runs covering the entire interfacial evolution (i.e., well past steady state) reveal that our results for the interfacial shape presented in this paper are accurate to at least 3 significant digits.

We emphasize that the computational investigation of capsules with shearing and area-dilatation resistance but negligible bending resistance in moderate and strong planar extensional flows is a well-posed problem while our spectral algorithm has been shown to describe very accurately complicated capsule shapes, as comparisons with experimental findings and other high-order algorithms have revealed [4,7,8].

To facilitate the description of our results, we imagine that the flow xy plane shown in Fig. 1 is vertical. Seeing the capsule from the positive z, y, or x axis represents a front, top, or side view, respectively. In addition, for a given capsule shape, we determine the three capsule dimensions (i.e., length L_x, width L_y, and depth L_z), as the maximum distance of the capsule surface in the x, y, and z coordinates, respectively, by employing a Newton method to solve the optimization problems using the spectral discretization points on the membrane. This is particular useful for the capsule width L_y which may occur not in the middle but in the dumbbell area of the capsule as discussed later.

III. STEADY-STATE CAPSULE PROPERTIES

A. Effects of flow nonlinearity

We start our investigation by presenting the steady-state capsule deformation as the flow nonlinearity strength is increased for membrane hardness $C = 1$. A negative flow nonlinearity b_A has a significant effect on the pressure field. Observe that for Antanovskii's extensional flow, at the capsule middle where $x = 0$, the undisturbed pressure is $p^\infty = p_0 + 6\mu G\, b_A(-y^2)/a^2 = p_0 + 6\mu G\, |b_A|\, y^2/a^2$; i.e., it increases with the flow nonlinearity strength $|b_A|$. At the capsule edges where $y = 0$, the undisturbed pressure is $p^\infty = p_0 - 6\mu G\, |b_A|\, x^2/a^2$; i.e., it decreases with the flow nonlinearity strength $|b_A|$.

The steady-state capsule shape for low flow nonlinearity $b_A = -0.05$ is shown in Fig. 2(a) for a high capillary number, $\mathrm{Ca} = 4$. The strong flow rate produces a large interfacial elongation but the decreased pressure at the capsule edges results in rounded capsule tips. In addition, the capsule middle is shortened at the xy plane owing to the local increased pressure of the nonlinear flow. Both

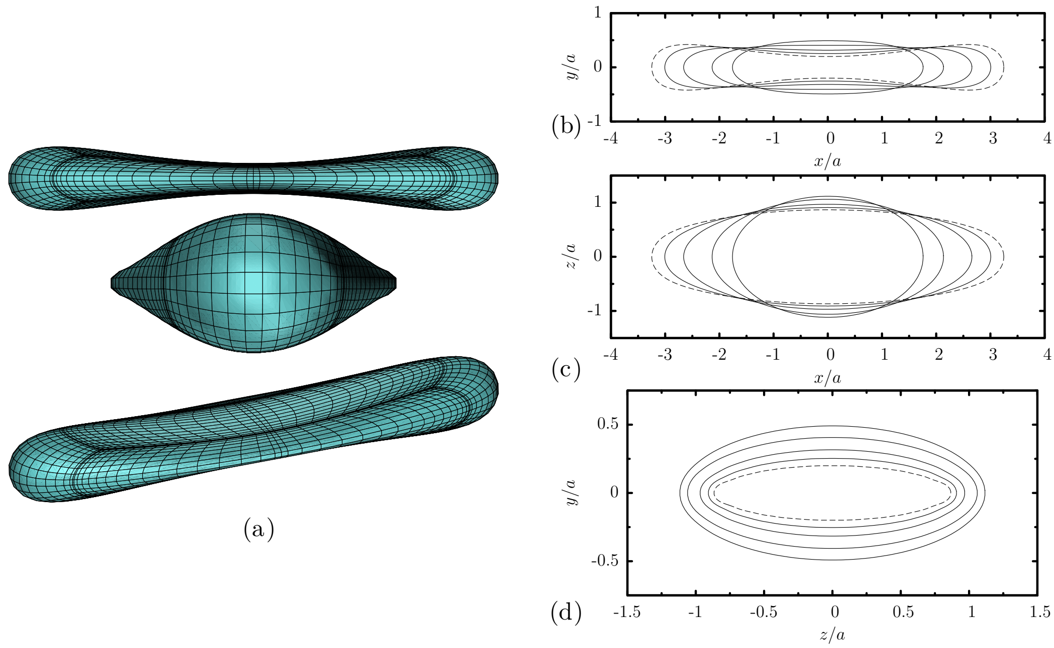

FIG. 2. Steady-state shape of a Skalak capsule with $C = 1$ and $b_A = -0.05$. (a) The capsule shape for $\mathrm{Ca} = 4$ plotted (from top to bottom) as seen from the positive z axis, the positive x axis, and slightly askew from the positive z axis to reveal the capsule's depth. The three-dimensional views are plotted based on the spectral grid using orthographic projection. [(b), (c), (d)] Steady-state profiles of a Skalak capsule with $C = 1$, $b_A = -0.05$ and $\mathrm{Ca} = 0.5, 1, 2, 3, 4$. (b) $z = 0$, (c) $y = 0$, and (d) $x = 0$ profile (i.e., interface intersection with the plane $z = 0$, $y = 0$ or $x = 0$, respectively).

effects result in the formation of a weak dumbbell. Owing to the flow field, the capsule obtains a fully three-dimensional shape while the side view from the x axis is pointed owing to the capsule middle cross section. The significant membrane hardness of $C = 1$ stabilizes the interfacial shape without the need for a large depth increase in the z direction, as seen in Fig. 2(c). These effects are more pronounced as the capillary number is increased as seen in the capsule profiles presented in Fig. 2.

In contrast, strong linear extensional flows extend significantly the capsule towards a slender configuration while the capsule edges become very pointed since the membrane tensions diminish in this area, as found in our earlier papers [4,8]. Thus, even a low flow nonlinearity effects the capsule shape significantly both in its middle and its edges, creating a different steady-state conformation than a linear extensional flow.

Increasing the flow nonlinearity to moderate values amplifies significantly the effects on the capsule conformation as shown in Fig. 3(a) for $b_A = -0.2$ and $\mathrm{Ca} = 3.5$. The increased pressure at the capsule middle creates a flat area there with small local width and thus the two sides of the membrane interface approach each other. At the same time, the capsule is only moderately extended along the x direction, as clearly shown in Fig. 3(b). Both effects result in the creation of a three-dimensional dumbbell with a flat and narrow middle which is pointed along the lateral z direction. [See the capsule's side view and profile in Figs. 3(a) and 3(d)].

The formation of the three-dimensional dumbbell shape with increasing capillary number is also shown in the capsule profiles of Fig. 3. Clearly these capsule conformations cannot be described by two-dimensional or axisymmetric models. The same is currently true by the view limitations in microfluidic channels which commonly permit only a front view corresponding to the capsule shape and profiles from the z axis seen in Figs. 3(a) and 3(b). Even the recent development of side

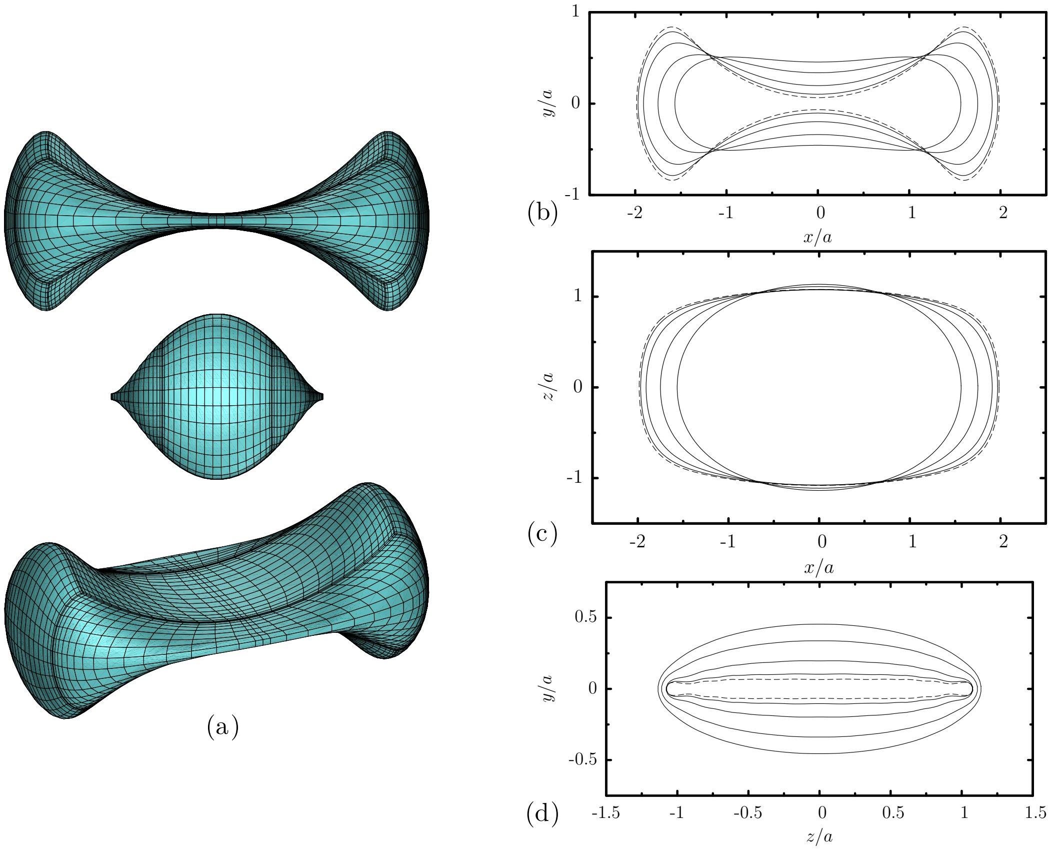

FIG. 3. Steady-state shape of a Skalak capsule with $C = 1$ and $b_A = -0.2$. (a) The capsule shape for $\mathrm{Ca} = 3.5$ plotted (from top to bottom) as seen from the positive z axis, the positive x axis, and slightly askew from the positive z axis to reveal the capsule's depth. [(b), (c), (d)] Steady-state profiles of a Skalak capsule with $C = 1$, $b_A = -0.2$ and $\mathrm{Ca} = 0.5, 1, 2, 3, 3.5$. (b) $z = 0$, (c) $y = 0$, and (d) $x = 0$ profile (i.e., interface intersection with the plane $z = 0$, $y = 0$, or $x = 0$, respectively).

views in microfluidic channels via prisms [20], which offers edge views as the one seen in Fig. 3(a), cannot capture the fully three-dimensional dumbbell shape presented in Fig. 3(a). Therefore, the experimental studies should monitor the capsule from several different view angles to capture the details of the three-dimensional interfacial shape.

High values of the flow nonlinearity result in a much more pronounced dumbbell formation, as seen in Fig. 4 for $b_A = -0.5$. In this case, the capsule does not practically elongate; instead it shows a large width extension in the dumbbell area as well as a significant lateral extension. The capsule middle is again flat and pointed in the lateral z direction. In essence, high flow nonlinearity causes the formation of a large three-dimensional dumbbell.

Figure 5 shows the evolution of the steady-state capsule shape for a high capillary number ($\mathrm{Ca} = 3$) as we increase the flow nonlinearity strength $|b_A|$ from very small values. For a linear extensional flow ($b_A = 0$) and this capillary number, the elongated and slender capsule is accompanied with pointed, cusped edges [8], as seen in the (front) $z = 0$ profile for the low flow nonlinearity $b_A = -0.01$ in Fig. 5(a). Increasing further the flow nonlinearity strength ($b_A = -0.02$), the capsule edges become rounded while the capsule remains slender. It requires a higher flow nonlinearity strength for the capsule middle to be shortened as shown in the $z = 0$ profile for $b_A = -0.04, -0.05$. The formation of the weak dumbbell is accompanied with a small decrease of the capsule length, which becomes

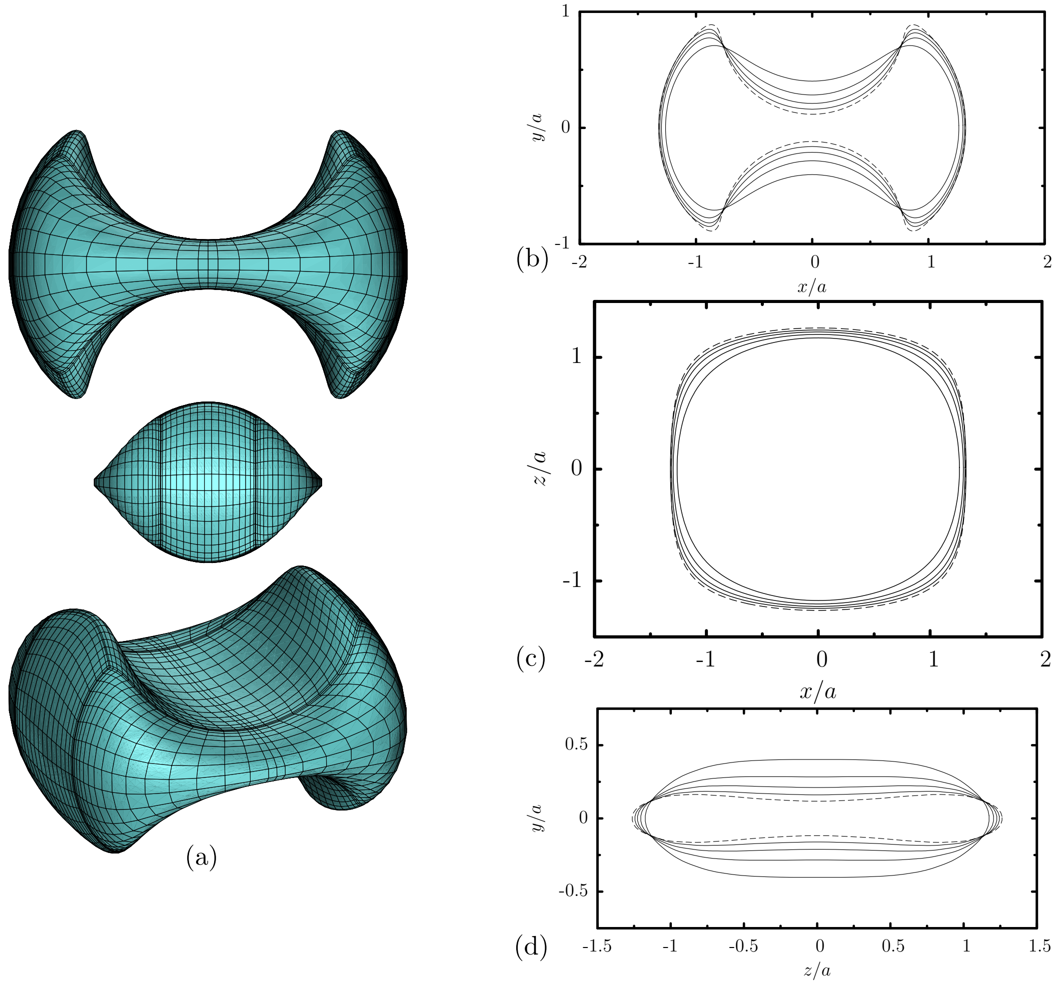

FIG. 4. Steady-state shape of a Skalak capsule with $C = 1$ and $b_A = -0.5$. (a) The capsule shape for $\mathrm{Ca} = 2.5$ plotted (from top to bottom) as seen from the positive z axis, the positive x axis, and slightly askew from the positive z axis to reveal the capsule's depth. [(b), (c), (d)] Steady-state profiles of a Skalak capsule with $C = 1$, $b_A = -0.5$ and $\mathrm{Ca} = 0.5, 1, 1.5, 2, 2.5$. (b) $z = 0$, (c) $y = 0$, and (d) $x = 0$ profile (i.e., interface intersection with the plane $z = 0$, $y = 0$, or $x = 0$, respectively).

more significant in much higher flow nonlinearity (e.g., $b_A = -0.1, -0.2$), where a large dumbbell is formed at steady state. At the same time, the capsule's (top) $y = 0$ profile remains elliptical with pointed edges at low flow nonlinearity and gradually becomes rectangular with rounded edges at higher flow nonlinearity, as seen in Fig. 5(b).

Therefore, the first action of a low flow nonlinearity at high capillary numbers is to transform the capsule edges from cusped to rounded. As the flow nonlinearity strength is further increased, the capsule edges become more rounded and its middle starts to shorten. The critical flow nonlinearity strength for the edge transition increases only slightly with the flow rate, from $b_A = -0.01$ for $\mathrm{Ca} = 2.5$ to $b_A = -0.02$ for $\mathrm{Ca} = 3,4$, for a capsule with membrane hardness $C = 1$.

We now turn our attention to the effects of the capillary number Ca on steady-state capsule properties describing both the overall and local deformation of the capsule, presented in Figs. 6 and 7. It is of interest to note that in these figures we do not present results for very low capillary numbers. In this case, near steady state, compressive tensions are developed on the capsule membrane, resulting in

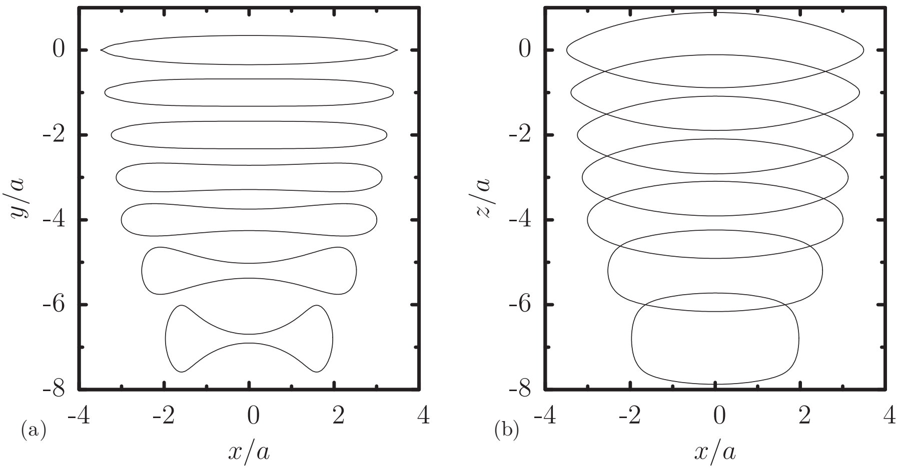

FIG. 5. Steady-state profiles of a Skalak capsule with $C = 1$, Ca $= 3$, and $b_A = -0.01, -0.02, -0.03, -0.04, -0.05, -0.1, -0.2$. (a) $z = 0$, and (b) $y = 0$ profile (i.e., interface intersection with the plane $z = 0$ and $y = 0$, respectively).

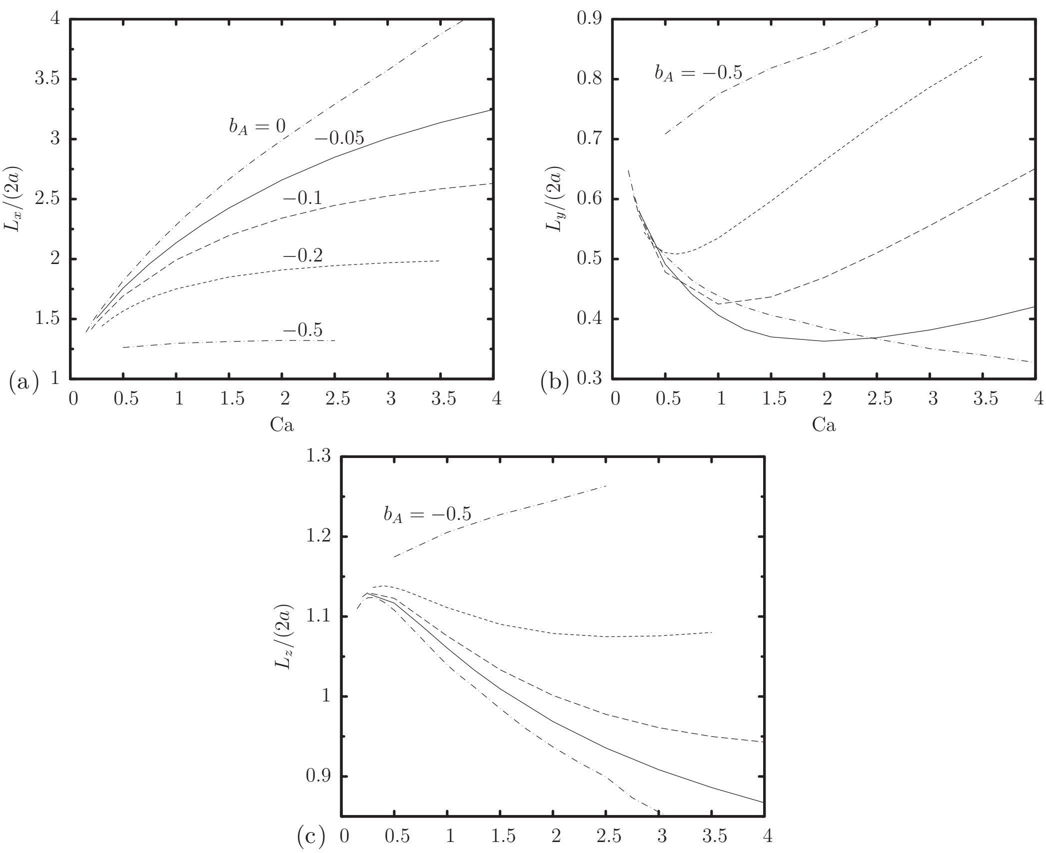

FIG. 6. Steady-state capsule's dimensions as a function of the capillary number Ca for a Skalak capsule with $C = 1$ and $b_A = 0, -0.05, -0.1, -0.2, -0.5$. (a) Length L_x, (b) width L_y, and (c) depth L_z.

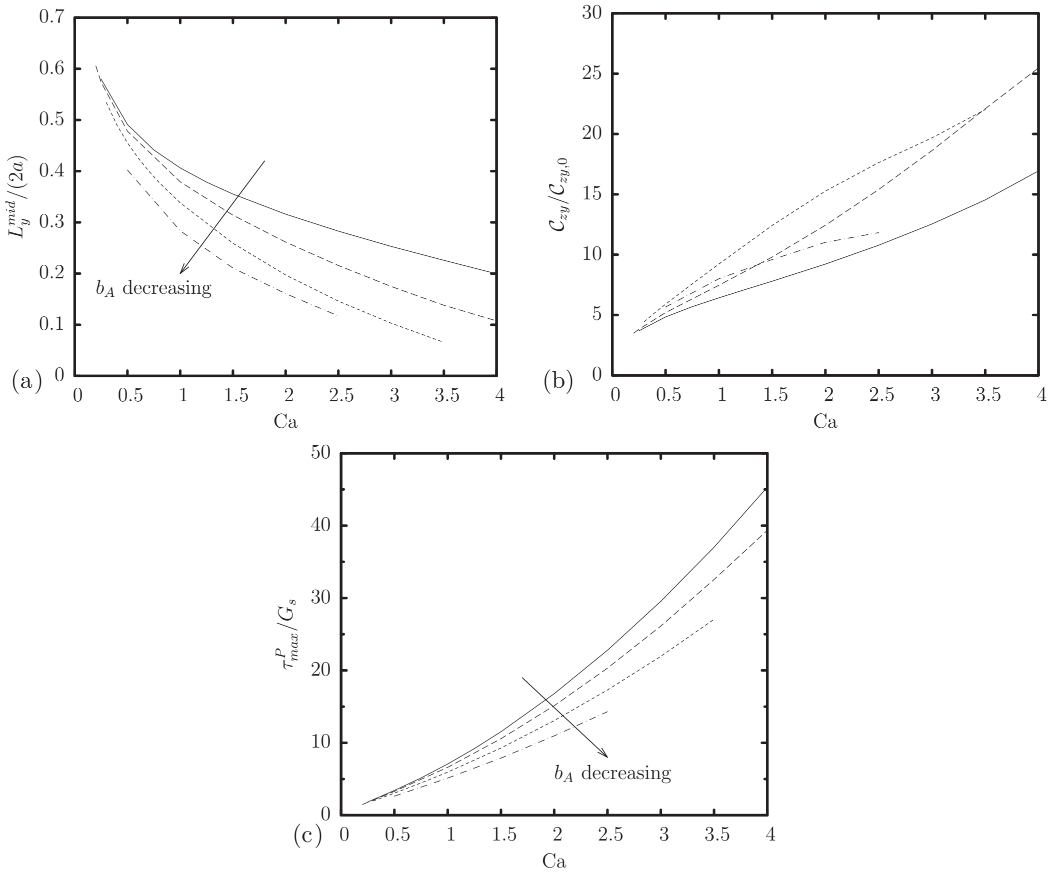

FIG. 7. Steady-state capsule properties as a function of the capillary number Ca for a Skalak capsule with $C = 1$ and $b_A = -0.05, -0.1, -0.2, -0.5$. (a) Middle width L_y^{mid}, (b) middle curvature $\mathcal{C}_{zy}$ scaled with the curvature of the quiescent spherical capsule $\mathcal{C}_{zy}^0 = a^{-1}$, and (c) maximum principal tension $\tau_{\max}^P$ among the spectral discretization points on the membrane.

wrinkling around the capsule equator and interfacial breaking for computational algorithms without sufficient bending resistance [4,5]. In addition, our computations show that for low flow nonlinearity $b_A = -0.05, -0.1$, the $C = 1$ capsules have a strong strain-hardening nature that enables them to withstand the highest flow rates in these extensional flows. However, for higher flow nonlinearity $b_A = -0.2, -0.5$, our computations are limited up to capillary number Ca $= 3.5, 2.5$, respectively. In strong flow nonlinearity, the capsule develops a very deformed three-dimensional dumbbell shape with a flat and pointed middle as shown in Figs. 3 and 4. Such shapes are very difficult to be computed numerically and thus we believe that the corresponding upper limit in Ca is of computational origin.

To quantify the overall deformation of the capsule, in Fig. 6 we present the three capsule dimensions, L_x, L_y, and L_z, i.e., the maximum distance of the capsule surface in the x, y, and z coordinates, respectively. The dependence of these lengths on the capillary number Ca for different values of b_A reveals clearly the two distinct capsule conformations we have identified in the earlier figures, i.e., the elongated shape with rounded edges at low flow nonlinearity b_A and the laterally extended dumbbell shape at high flow nonlinearity.

As shown in Fig. 6(a), for a given capillary number, the capsule length L_x is decreased with the flow nonlinearity strength $|b_A|$, owing to the smaller hydrodynamics forces associated with the cubic term in the flow field (1). In essence, for Antanovskii's flow the effective capillary number scales as

$$\mathrm{Ca}^{\mathrm{eff}} = f_\mu\, a/G_s \sim \mathrm{Ca}\,(1+b_A) \sim \mathrm{Ca}\,(1-|b_A|) \tag{4}$$

if we consider that the deforming normal stress of the external fluid exerted on the capsule membrane scales as $f_\mu \sim \mu\, \partial u_x^\infty/\partial x \sim \mu\, G\,(1+b_A)$.

For low and moderate flow nonlinearity, e.g., $b_A = -0.05, -0.1, -0.2$, the capsule width L_y initially decreases with the capillary number Ca as seen in Fig. 6(b), owing to the flow impact at the top and bottom of the capsule middle, where the width L_y is located. As the capillary number increases, the capsule width is increased owing to the dumbbell formation. Therefore, in Fig. 6(b), the minimum width L_y denotes the change of the width location from the capsule middle for low Ca to the dumbbell area for higher Ca. For the high flow nonlinearity $b_A = -0.5$ and the flow rates studied in this work, the capsule width is located in the dumbbell area, and thus it is continuously increased with the capillary number Ca owing to the formation of a larger dumbbell shape.

The two distinct capsule conformations are also shown in the behavior of the capsule depth L_z presented in Fig. 6(c). For low flow nonlinearity b_A, the capsule depth L_z is continuously decreased with the capillary number Ca to accommodate the associated increase of the capsule length L_x owing to the capsule's volume preservation. The decrease of the capsule depth L_z with Ca is smaller as the flow nonlinearity strength $|b_A|$ increases owing to the smaller length extension of the capsule. For the high flow nonlinearity $b_A = -0.5$, the capsule length L_x is practically independent of the capillary number, a large dumbbell is formed with a narrow middle, and thus the capsule depth L_z is monotonically increased with Ca to accommodate the constant capsule volume.

To quantify the capsule local deformation at its middle, in Fig. 7 we present the middle width L_y^{mid}, the middle curvature $\mathcal{C}_{zy}$, and the maximum principal tension $\tau_{\max}^P$. Note that L_y^{mid} is the width of the capsule's $z=0$ profile for $x=0$; e.g., see Fig. 3(b). As the flow nonlinearity strength $|b_A|$ and the capillary number Ca increase, the increased pressure at the capsule middle $p^\infty = p_0 + 6\mu G\,|b_A|\,y^2/a^2$, where $p_0 \sim \mu G$ or

$$p^\infty/(G_s/a) \sim \mathrm{Ca}\,(1+|b_A|) \tag{5}$$

causes a narrower middle and thus the middle width L_y^{mid} is significantly reduced as shown in Fig. 7(a).

Figure 7(b) shows the dependence of the middle curvature $\mathcal{C}_{zy}$ on the flow nonlinearity b_A and the capillary number Ca. Observe that $\mathcal{C}_{zy}$ is a line curvature determined along the capsule's $x=0$ profile at $y=0$ [e.g., see Fig. 3(d)], and thus it is used to quantify the capsule's pointed middle along the lateral z direction. As the capillary number increases, the increased interfacial deformation causes a very pointed capsule middle for any flow nonlinearity, and thus the appearance of a local length scale there which is much smaller than the capsule size. In essence, while a strong linear extensional flow creates elongated capsule shapes with pointed edges [4,8], the nonlinear extensional flows studied in this work form a pointed capsule middle at high flow rates.

Figure 7(c) shows the dependence on the flow nonlinearity b_A and the capillary number Ca of the maximum principal tension $\tau_{\max}^P$ among the spectral discretization points on the membrane. The maximum tension at steady state occurs at the intersection of the capsule's surface with the z axis, i.e., the location of the capsule depth L_z, and points in the direction of the capsule elongation. (This is also the location of $\tau_{\max}^P$ during the transient capsule evolution from the quiescent spherical shape.) Being the maximum tension, $\tau_{\max}^P$ is associated with the capsule's overall deformation; i.e., as the capillary number is increased, the hard-straining membrane develops strong tensions needed to stabilize the large capsule deformation. For a given capillary number, the maximum tension $\tau_{\max}^P$ is increased as the flow nonlinearity strength $|b_A|$ decreases, owing to the associated larger overall interfacial deformation as seen in the increased capsule length L_x in Fig. 6 and the membrane surface area S_c (not shown). Since $\tau_{\max}^P$ always occurs at a specific membrane location, it also characterizes the large local deformation at the capsule's pointed middle area. Furthermore, this location is the most probable to rupture due to excessive tensions in extensional flows.

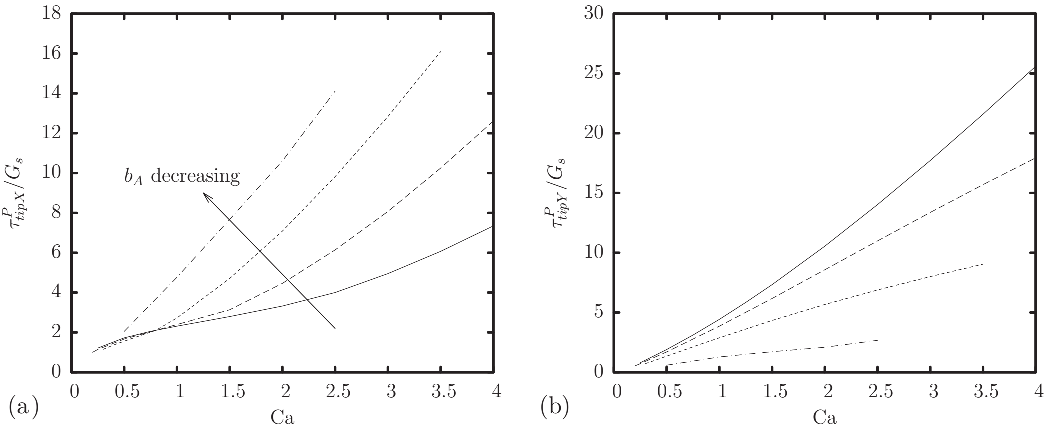

FIG. 8. Steady-state capsule properties as a function of the capillary number Ca for a Skalak capsule with $C = 1$ and $b_A = -0.05, -0.1, -0.2, -0.5$. (a) Maximum principal tension $\tau^P_{\text{tip}X}$, and (b) maximum principal tension $\tau^P_{\text{tip}Y}$.

It is of interest to note that significant tensions are also developed at the capsule edges and its top (or bottom) middle area as shown in Fig. 8. Note that the x tip is the capsule edge, i.e., the intersection of the capsule's surface with the x axis while the y tip is the intersection of the capsule's surface with the y axis at the capsule top middle area. At both locations, significant tensions are developed owing to the increased local interfacial deformation. At the capsule edges, the dumbbell is more pronounced for higher flow nonlinearity and thus $\tau^P_{\text{tip}X}$ increases with the flow nonlinearity strength $|b_A|$. At the y tip, the capsule elongation along the x axis, i.e., the capsule length L_x, is increased at low flow nonlinearity, and thus $\tau^P_{\text{tip}Y}$ decreases with the flow nonlinearity strength $|b_A|$ as seen in Fig. 8.

We conclude this section by providing a shape diagram for the steady-state capsule shown in Fig. 9. In this figure, the transition from an elongated shape to a weak dumbbell occurs when the

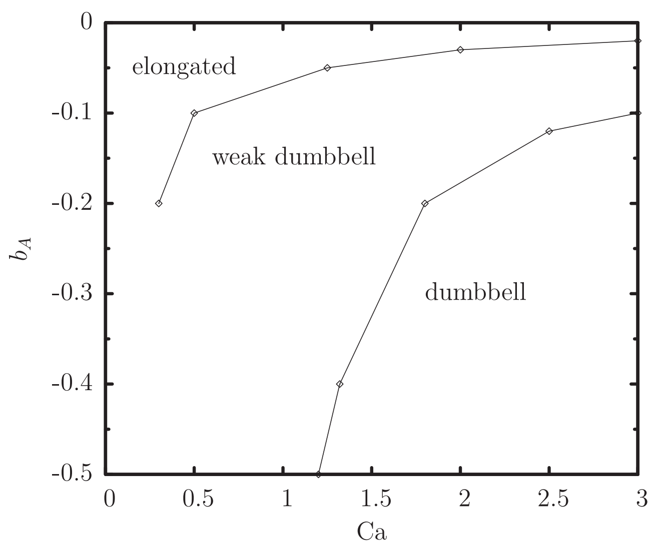

FIG. 9. Shape diagram for a Skalak capsule with $C = 1$ at steady state, as a function of the capillary number Ca and the flow nonlinearity b_A.

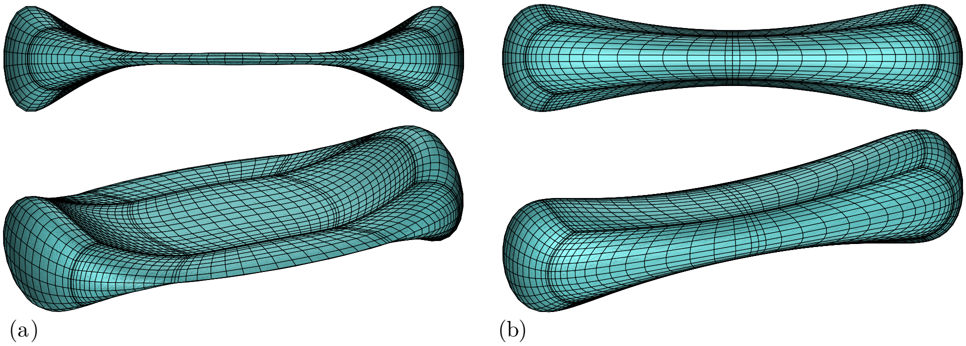

FIG. 10. Steady-state shape of a Skalak capsule with $b_A = -0.1$ for (a) $C = 0.1$, Ca $= 3$, and (b) $C = 5$, Ca $= 5$, as seen from the positive z axis and slightly askew from it to reveal the capsule's depth.

capsule's middle width L_y^{mid} decreases to the value of the capsule width L_y (i.e., $L_y^{\mathrm{mid}} = L_y$), while the transition from a weak dumbbell to a well-established dumbbell occurs when $L_y^{\mathrm{mid}} = 0.3L_y$. [These transition limits are motivated by the capsule profiles shown earlier in Fig. 5(a).]

B. Effects of membrane hardness

We consider now the effects of the membrane hardness C for a typical flow nonlinearity, $b_A = -0.1$. As shown in Fig. 10, at strong flows the less strain-hardening capsule with $C = 0.1$ develops a three-dimensional dumbbell shape with a flat extended middle which resembles a long straight neck along the $z = 0$ profile. On the other hand, the more strain-hardening capsule with $C = 5$ develops a axisymmetric-like weak dumbbell shape and thus its shape remains cylindrical-like with rounded edges even at strong flows with Ca $= 5$.

The distinct capsule conformations at low and high membrane hardness C are shown clearly in Fig. 11 where we present the $z = 0$ and $y = 0$ profiles for different hardness, $C = 0.1, 1, 5$, at the same capillary number Ca $= 3$. Observe that the less strain-hardening capsule elongates significantly along the lateral z direction which results in a higher surface area increase at a given capillary number.

As revealed by our analysis on similar deformation patterns in linear extensional flows [7], the less strain-hardening capsules tend to become flat and extended along the lateral direction so that they can increase their area-dilatation resistance (owing to the higher surface area increase) and thus are able to withstand the strong hydrodynamic forces at high capillary numbers. In contrast, the more strain-

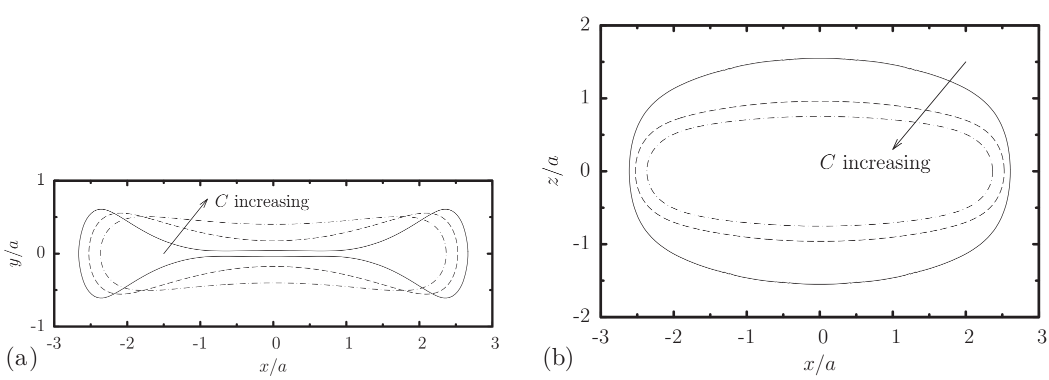

FIG. 11. Steady-state profiles of a Skalak capsule with $C = 0.1, 1, 5$, $b_A = -0.1$, and Ca $= 3$. (a) $z = 0$ profile and (b) $y = 0$ profile.

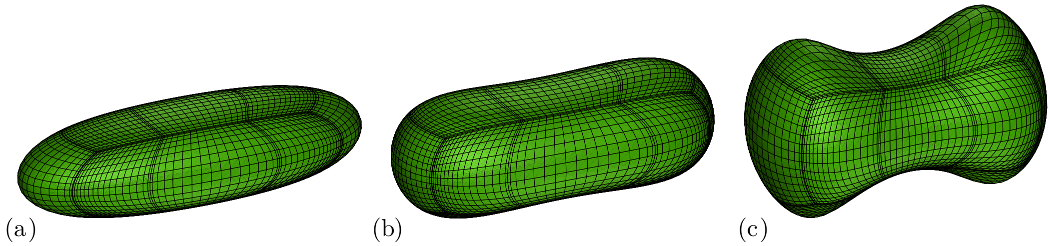

FIG. 12. Steady-state shape of a droplet with $\lambda = 0$ as seen slightly askew from the z axis to reveal the droplet depth. (a) $b_A = -0.05$ and $\mathrm{Ca} = 0.22$, (b) $b_A = -0.2$ and $\mathrm{Ca} = 0.22$, and (c) $b_A = -0.5$ and $\mathrm{Ca} = 0.32$.

hardening capsules are stabilized mainly via the membrane's shearing resistance while their high membrane hardness keep their elongated shape axisymmetric-like even at strong extensional flows.

C. Comparison with droplets dynamics

Our investigation has revealed that strain-hardening capsules obtain very deformed three-dimensional dumbbell shapes at steady state by developing strong membrane tensions, and thus being able to withstand strong flow rates in the nonlinear extensional flows studied in this work. To highlight the strong stability properties of these capsules, we compare them now with the dynamics of droplets with constant surface tension.

To determine the droplet dynamics, we utilized both our explicit and the fully implicit time-integration spectral boundary element algorithms for droplets [24,25]. In this case, the capillary number is defined as $\mathrm{Ca} = \mu Ga/\gamma$, where γ is the droplet's constant surface tension. In addition, the viscosity ratio λ does affect the droplet shape even at steady state owing to the inner circulation. As the viscosity ratio λ increases, the droplet deformation increases owing to the higher inner hydrodynamic forces. Since our droplet results for $\lambda = 0,1,5$ are qualitatively similar, we only present our results for the $\lambda = 0$ droplets, which correspond better to the capsule shapes at steady state owing to the zero inner circulation.

Figure 12 shows the steady-state shapes of an inviscid droplet (i.e., a bubble) at the highest capillary number we were able to obtain a steady-state deformation for flow nonlinearity $b_A = -0.05, -0.2, -0.5$. For low and moderate flow nonlinearity $b_A = -0.05, -0.2$, the droplet middle has shortened only slightly while the droplet practically resembles an axisymmetric-like rod with rounded edges. Only for the high flow nonlinearity $b_A = -0.5$ has a weak dumbbell been formed. Owing to the constant surface tension γ (i.e., along both the flow and lateral directions), the droplet shape in all cases resembles more that of capsules of high membrane hardness $C = 5$ at low capillary numbers.

For $b_A = -0.2$, when we increase the capillary number to $\mathrm{Ca} = 0.23$, the droplet is unable to reach steady state; instead it deforms continuously, obtaining a dumbbell shape, and eventually breaks at its middle. [The transient droplet profiles resemble the steady-state capsule profiles with increasing capillary number shown in Fig. 3(b).] We emphasize that we obtain similar deformation behavior for equiviscous and high-viscosity droplets with $\lambda = 1,5$ which are able to reach steady state up to capillary number $\mathrm{Ca} = 0.17, 0.15$, respectively for this flow nonlinearity.

Thus, droplets with a constant surface tension are unable to withstand strong nonlinear extensional flows and thus they cannot achieve the highly deformed steady-state dumbbell shapes of strain-hardening capsules in these flows. This contrast significantly with the ability of bubbles to reach very deformed steady-state slender shapes with pointed edges in linear extensional flows [17,19].

IV. MULTILENGTH TRANSIENT CAPSULE DYNAMICS

We now turn our attention to the transient capsule dynamics to present an additional issue associated with the multiple length-scale physics of large capsule deformations.

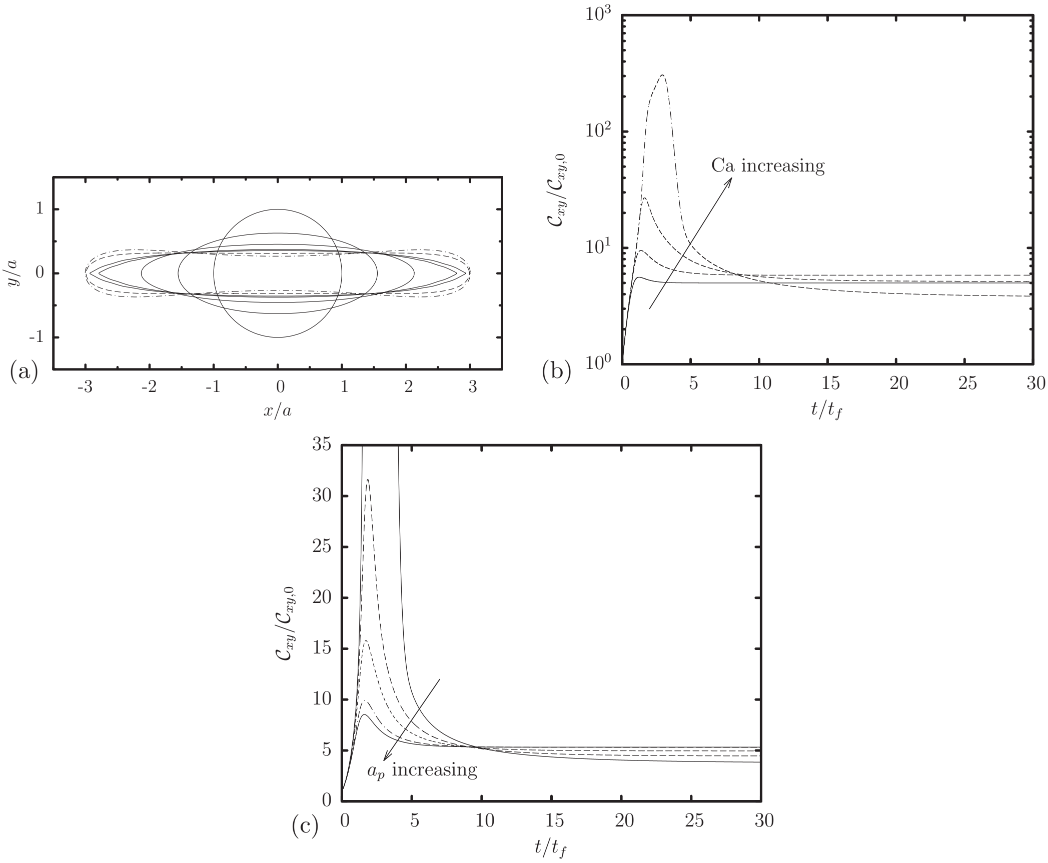

FIG. 13. Evolution of a Skalak capsule with $C = 1$ and $b_A = -0.05$, starting from a spherical shape. (a) $z = 0$ profile (i.e., interface intersection with the plane $z = 0$) for Ca = 3 and time $t/t_f = 0, 0.5, 1, 2, 3, 8, 100$. (b) Edge curvature $\mathcal{C}_{xy}$ for Ca = 0.5, 1, 2, 3. (c) Edge curvature $\mathcal{C}_{xy}$ for Ca = 3 and prestress $a_p = 0, 0.05, 0.1, 0.17, 0.2$. (Note that our computations cover times up to $t/t_f = 100$, where $t_f = G^{-1}$ is the flow time scale.)

Figure 13(a) shows the evolution of the $z = 0$ profile of a capsule in a strong flow with Ca = 3 at low flow nonlinearity $b_A = -0.05$, starting from the quiescent shape until the steady state is well established. Clearly the capsule edges become very pointed during the transient deformation and then gradually become rounded towards steady state. The transient overshooting in the edge curvature $\mathcal{C}_{xy}$ is increased with the capillary number, and can be two orders of magnitude higher than the steady-state value in strong flows as seen in Fig. 13(b).

The transient curvature overshooting was first identified in our earlier papers on the capsule dynamics in linear extensional flows [4,8] and it associated with the fact that at the quiescent equilibrium shape the membrane does not have any tensions. When placing the capsule in a strong flow, initially the membrane tensions are weak and thus are unable to stabilize the strong deforming hydrodynamics forces. This results in pointed capsule edges where the large local curvature contributes to the interfacial stabilization. After some time, the membrane tensions increase (owing to the increased capsule deformation) and cause a decrease in the edge curvature towards its steady-state value. Thus, for strain-hardening Skalak capsules in strong flows, the maximum value of the edge curvature during the transient evolution can be several times higher than its steady-state value.

To investigate this issue more, we studied the effects of the capsule prestress. As fabricated, artificial capsules may be slightly overinflated and thus prestressed. As in our earlier papers, we define the prestress parameter α_p such that all lengths in the undeformed capsule would be scaled by $(1+\alpha_p)$, relative to the reference shape [26,27]. Since the capsule is initially spherical, its membrane is initially prestressed by an isotropic elastic tension $\tau_0 = \tau_\beta^P(t=0)$ which depends on the employed constitutive law and its parameters but not on the capsule size. For example, for a Skalak capsule with $C = 1$ and $\alpha_p = 0.05$, the undisturbed capsule size a is 5% higher than that of the reference shape and the initial membrane tension owing to prestress is $\tau_0/G_s \approx 0.3401$; for $\alpha_p = 0.2$ the initial membrane tension is $\tau_0/G_s \approx 1.984$.

Figure 13(c) shows that by increasing the capsule prestress, the transient curvature overshooting is reduced since the initial membrane tensions are stronger and thus able to withstand better the deforming hydrodynamics forces. Thus, the transient curvature overshooting is a pure hydrodynamic effect of the growth of the membrane tensions with the interfacial deformation, and it occurs even for low negative flow nonlinearity associated with rounded steady-state capsule edges. It is of interest to mention that the edges of a real capsule may be probable to rupture owing to the transient curvature overshooting and thus the appearance of a small local length scale there.

We conclude this section by mentioning that we also investigated the dynamics of capsules made of strain-softening neo-Hookean membranes. (For the definition of this membrane type, please see our earlier paper [4].) As we found for linear extensional flows [7], these capsules show similar deformation behavior with the less strain-hardening Skalak capsules. Owing to their strain-softening nature, the neo-Hookean capsules cannot withstand high flow rates while they tend to become flat to increase their area-dilatation resistance [7]. For the nonlinear flows studied in this work, our computations reveal that the neo-Hookean capsules show a small transient curvature overshooting since they can withstand only moderate flow rates.

V. CONCLUSIONS

In this paper, we have investigated computationally the dynamics of an elastic capsule made of a strain-hardening membrane in planar extensional Stokes flows where the velocity is a nonlinear (i.e., cubic) function of position associated with a decreased pressure at the particle edges and an increased pressure at the particle middle. Such flows may be generated in cross-slot and four-roll-mill microdevices owing to the solid boundaries.

Studying the flow-induced deformation of soft particles provides useful information on the utilization of these particles in chemical, pharmaceutical, and physiological processes. For example, understanding the stability of soft particle shapes provides helpful insight into the hydrodynamic aggregation and the effective viscosity of suspensions [28]. The deformation of artificial capsules in microchannels is directly associated with drug delivery, cell sorting, and cell characterization [29,30]. The flow-induced deformation of soft particles is determined by the nonlinear coupling of the deforming hydrodynamic forces with the restoring interfacial forces of the particle membrane. Since the latter forces depend on the type of the soft-particle interface, this suggests that different soft particles (such as droplets, artificial capsules, and cells) may obtain quite different shapes.

Our investigation has revealed that in strong flow rates of the nonlinear extensional flows studied in this work, strain-hardening capsules obtain very deformed three-dimensional dumbbell shapes at steady state by developing strong membrane tensions. In addition, we have identified two distinct steady-state capsule conformations, i.e., an elongated weak dumbbell shape with rounded edges at low flow nonlinearity and a laterally extended dumbbell shape at high flow nonlinearity. These effects are more pronounced for the less strain-hardening capsules which develop a flat extended middle where the two sides of the membrane approach each other.

On the other hand, droplets with a constant surface tension at any viscosity ratio are unable to withstand strong nonlinear extensional flows and thus they cannot achieve the highly deformed steady-state dumbbell shapes of strain-hardening capsules in these flows. This contrasts significantly with the ability of low-viscosity droplets (or bubbles) to reach very deformed steady-state slender shapes with pointed edges in linear extensional flows [17,19].

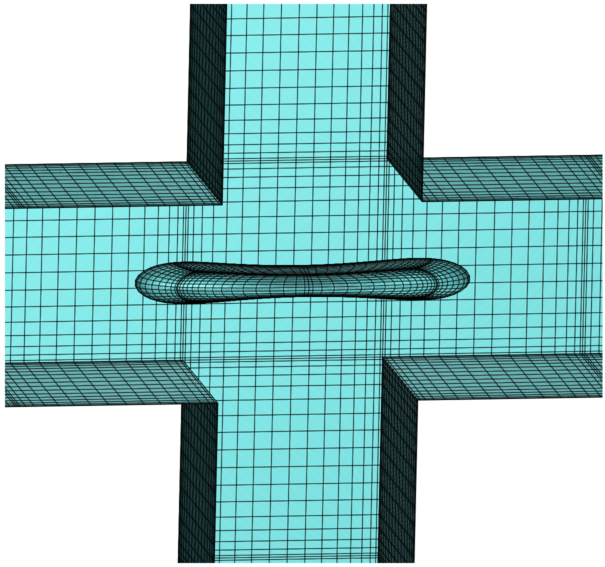

FIG. 14. Steady-state shape of a Skalak capsule with $C = 1$ at the stagnation point of a microfluidic cross junction constructed by two square channels of half-length ℓ_z. The capsule size is $a/\ell_z = 0.5$ and the channel's capillary number is $\mathrm{Ca} = \mu\mathcal{U}/G_s = 2$, where $\mathcal{U}$ is the average velocity in each of the two square channels of the cross junction.

Starting from the quiescent spherical shape, an elastic capsule in strong flow rates at low flow nonlinearity first develops very pointed edges which become rounded towards steady state. Our study shows that the transient curvature overshooting is a pure hydrodynamic effect of the growth of the membrane tensions with the interfacial deformation, and thus it is reduced when the capsule prestress increases.

Our investigation has revealed two probable locations for membrane rupture of a real capsule in extensional flows, i.e., the capsule edges owing to the transient curvature overshooting and the lateral pointed capsule middle owing to excessive tensions.

To show the association of our study with the extensional flows generated in microfluidic devices, we investigated the capsule dynamics in a microfluidic cross junction constructed by two square channels. As seen in Fig. 14, the steady-state shape of a capsule with size smaller but comparable to the channel size clearly corresponds to a flow nonlinearity b_A in the interval $[-0.10, -0.05]$. The flow nonlinearity generated in a cross junction increases with the capsule size and also depends on the exact shape of the junction, e.g., if the device has sharp or rounded corners and the aspect ratio of the rectangular channels comprising the junction.

The complicated three-dimensional dumbbell shapes of elastic capsules in the nonlinear extensional flows studied in this work cannot be described by two-dimensional or axisymmetric models, or via front and side views in microfluidic channels. Therefore, we hope that our study motivates for more experiments with elastic capsules in nonlinear extensional flows; in such case the experimental studies should monitor the capsules from different view angles to capture the details of the three-dimensional interfacial shapes.

ACKNOWLEDGMENTS

This work was supported in part by the National Science Foundation. Some computations were performed on multiprocessor computers provided by the Extreme Science and Engineering Discovery Environment (XSEDE).

[1] *Modeling and Simulation of Capsules and Biological Cells*, edited by C. Pozrikidis (Chapman and Hall, London, 2003).
[2] A. S. Popel and P. C. Johnson, Microcirculation and hemorheology, Annu. Rev. Fluid Mech. **37**, 43 (2005).
[3] K. S. Chang and W. L. Olbricht, Experimental studies of the deformation of a synthetic capsule in extensional flow, J. Fluid Mech. **250**, 587 (1993).
[4] W. R. Dodson III and P. Dimitrakopoulos, Dynamics of strain-hardening and strain-softening capsules in strong planar extensional flows via an interfacial spectral boundary element algorithm for elastic membranes, J. Fluid Mech. **641**, 263 (2009).
[5] E. Lac, D. Barthès-Biesel, N. A. Pelekasis, and J. Tsamopoulos, Spherical capsules in three-dimensional unbounded Stokes flows: effect of the membrane constitutive law and onset of buckling, J. Fluid Mech. **516**, 303 (2004).
[6] P. M. Vlahovska, Y.-N. Young, G. Danker, and C. Misbah, Dynamics of a non-spherical microcapsule with incompressible interface in shear flow, J. Fluid Mech. **678**, 221 (2011).
[7] P. Dimitrakopoulos, Effects of membrane hardness and scaling analysis for capsules in planar extensional flows, J. Fluid Mech. **745**, 487 (2014).
[8] W. R. Dodson III and P. Dimitrakopoulos, Spindles, Cusps, and Bifurcation for Capsules in Stokes Flow, Phys. Rev. Lett. **101**, 208102 (2008).
[9] P. Dimitrakopoulos, Cusp formation for capsules in nonlinear extensional Stokes flows (unpublished).
[10] F. J. Galindo-Rosales, M. A. Alves, and M. S. N. Oliveira, Microdevices for extensional rheometry of low viscosity elastic liquids: A review, Microfluid Nanofluid **14**, 1 (2013).
[11] S. D. Hudson, F. R. Phelan, Jr., M. D. Handler, J. T. Cabral, K. B. Migler, and E. J. Amis, Microfluidic analog of the four-roll mill, Appl. Phys. Lett. **85**, 335 (2004).
[12] J. S. Lee, R. Dylla-Spears, N. P. Teclemariam, and S. J. Muller, Microfluidic four-roll mill for all flow types, Appl. Phys. Lett. **90**, 074103 (2007).
[13] M. Tanyeri and C. M. Schroeder, Manipulation and confinement of single particles using fluid flow, Nano Lett. **13**, 2357 (2013).
[14] L. K. Antanovskii, A plane inviscid incompressible bubble placed within a creeping viscous flow: Formation of a cusped bubble, Eur. J. Mech. B **13**, 491 (1994).
[15] C. Pozrikidis, Numerical studies of cusp formation at fluid interfaces in Stokes flow, J. Fluid Mech. **357**, 29 (1998).
[16] L. K. Antanovskii, Formation of a pointed drop in Taylor's four-roller mill, J. Fluid Mech. **327**, 325 (1996).
[17] G. I. Taylor, The formation of emulsions in definable fields of flow, Proc. Roy. Soc. London, Ser. A **146**, 501 (1934).
[18] D. Barthès-Biesel, Role of interfacial properties on the motion and deformation of capsules in shear flow, Phys. A (Amsterdam, Neth.) **172**, 103 (1991).
[19] B. J. Bentley and L. G. Leal, An experimental investigation of drop deformation and breakup in steady two-dimensional linear flows, J. Fluid Mech. **167**, 241 (1986).
[20] C. de Loubens, J. Deschamps, G. Boedec, and M. Leonetti, Stretching of capsules in an elongation flow: A route to constitutive law, J. Fluid Mech. **767**, R3 (2015).
[21] M. Rachik, D. Barthès-Biesel, M. Carin, and F. Edwards-Levy, Identification of the elastic properties of an artificial capsule membrane with the compression test: Effect of thickness, J. Colloid Interface Sci. **301**, 217 (2006).
[22] R. Skalak, A. Tozeren, R. P. Zarda, and S. Chien, Strain energy function of red blood cell membranes, Biophys. J. **13**, 245 (1973).
[23] S. Timoshenko and S. Woinowsky-Krieger, *Theory of Plates and Shells*, 2nd ed. (McGraw-Hill, New York, 1959).
[24] P. Dimitrakopoulos, Interfacial dynamics in Stokes flow via a three-dimensional fully-implicit interfacial spectral boundary element algorithm, J. Comp. Phys. **225**, 408 (2007).
[25] Y. Wang and P. Dimitrakopoulos, Low-Reynolds-number droplet motion in a square microfluidic channel, Theor. Comput. Fluid Dyn. **26**, 361 (2012).

[26] S. Kuriakose and P. Dimitrakopoulos, Motion of an elastic capsule in a square microfluidic channel, Phys. Rev. E **84**, 011906 (2011).

[27] S.-Y. Park and P. Dimitrakopoulos, Transient dynamics of an elastic capsule in a microfluidic constriction, Soft Matter **9**, 8844 (2013).

[28] G. Coupier, A. Farutin, C. Minetti, T. Podgorski, and C. Misbah, Shape Diagram of Vesicles in Poiseuille Flow, Phys. Rev. Lett. **108**, 178106 (2012).

[29] M. Abkarian, M. Faivre, R. Horton, K. Smistrup, C. A. Best-Popescu, and H. A. Stone, Cellular-scale hydrodynamics, Biomed. Mater. **3**, 034011 (2008).

[30] A. Alexeev and A. C. Balazs, Designing smart systems to selectively entrap and burst microcapsules, Soft Matter **3**, 1500 (2007).